Unsteady Stagnation Point Flow of Mass and Heat Transfer over a Stretching/Shrinking Sheet with Suction or Injection

SINDI M. CHIGOZIE[1], RAPHAEL E. ASIBOR[2], AKINDELE M. OKEDOYE[3]
[1] *Department of Mathematics, College of Science, Federal University of Petroleum Resources, Effurun, Nigeria*
[2] *Department of Computer Science/Mathematics, Igbinedion University Okada, Edo State, Nigeria*
[3] *Department of Mathematics, College of Science and Technology, Covenant University, Ota, Nigeria*

Abstract*—The interest in this work is due to the many practical applications which can be modeled or approximated. as transport phenomena in porous media. We consider the impacts of unsteady stagnation point flow of mass and heat transfer over a stretching/shrinking sheet with suction or injection in a stretchable porous device. The higher order nonlinear partial differential equations are converted into first order simultaneous linear differential equations using suitable similarity variables and then transformed to initial value problem. and are solved numerically using Runge–Kuta fourth order method along with shooting technique. The solution for the non-magnetic and buoyancy case is chosen as an initial guess and the iterations using Euler scheme are continued till convergence within prescribed accuracy is achieved, with the corrections incorporated in subsequent iterative steps until convergence, which is used to obtain the values of our initial guesses. As a result of the numerical calculations, the velocity, temperature and chemical species distributions for the flow are obtained and are displayed in figures and tables for different values flow governing parameters. From the result obtained it was observed that thermal Grashof number and buoyancy ratio aided the velocity for cooling problem while unsteadiness parameter increases the velocity distribution. Other emerging parameters were presented and discussed.

Indexed Terms*—Runge–Kutta, stagnation point, heat transfer, transport phenomena, porous media, shooting, stagnation point flow.

I. INTRODUCTION

Convective flows in porous media have been extensively studied during the last several decades, and they have included several different physical effects. This interest is due to the many practical applications which can be modeled or approximated. as transport phenomena in porous media. These flows appear in a wide variety of industrial applications, as well as in many natural circumstances such as geothermal extraction, storage of nuclear waste material, ground water flows, industrial and agricultural water distribution, oil recovery processes, thermal insulation engineering, pollutant dispersion in aquifers, cooling of electronic components, packed-bed reactors, food processing, casting and welding of manufacturing processes, the dispersion of chemical contaminants in various processes in the chemical industry and in the environment, soil pollution, fibrous insulation and even for obtaining approximate solutions for flow through turbo-machinery. Theories and experiments of thermal convection in porous media and the state-of-the-art reviews, with special emphasis on practical applications have been presented in the recent books by Ingham and Pop [1] and Nield and Bejan [2]. Fluid properties and its usefulness can be improved by magnetic induction that create electrical conductivity of the fluid, and have been applied in magnetohydromagnetic (MHD) power generators, nuclear reactors, heatexchangers and many other processes Okedoye [3].Moreover, the magnetohydrodynamic (MHD) rotating fluids in the presence of a magnetic field are encountered in many important problems in geophysics, astrophysics, and cosmical and geophysical fluid dynamics. It can provide explanations for the observed maintenance and secular variations of the geomagnetic field. It is also relevant in the solar physics involved in the

sunspot development, the solar cycle, and the structure of rotating magnetic stars. The effect of the Coriolis force due to the Earth's rotation is found to be significant as compared to the inertial and viscous forces in the equations of motion. The Coriolis and electromagnetic forces are of comparable magnitude, the former having a strong effect on the hydromagnetic flow in the Earth's liquid core, which plays an important role in the mean geomagnetic field. Several investigations are carried out on the problem of hydrodynamic flow of a viscous incompressible fluid in rotating medium considering various variations in the problem. Mention may be made of the studies of Ahmed and Sajid [4], Khan and Ellahi [5], Abelman et al. [6], Ellahi et al. [7], Hayat et al. [8], Husain et al. [9] and Hayat et al. [10]. Hayat et al. [11] analyzed the effects of Hall current on unsteady flow of a second-grade fluid in a rotating system. Hayat and Mumtaz [12] have examined the resonant oscillations of a plate in an electrically conducting rotating Johnson–Segalman fluid. Hayat [13] has presented the modeling and exact analytic solutions for hydromagnetic oscillatory rotating flows of a Burger's fluid. Abbas et al. [14] studied the unsteady MHD boundary layer flow and heat transfer analysis in an incompressible rotating viscous fluid over a stretching continuous sheet. The problem of free convection heat with mass transfer for MHD non-Newtonian Eyring–Powell flow through a porous medium, over an infinite vertical plate is studied by Eldabe et al. [15]. Mohamed and Ahmed [16] reported influences of Slip Velocity and Induced Magnetic Field on MHD Stagnation-Point Flow and Heat Transfer of Casson Fluid over a Stretching Sheet while Andersson et al. 17 presented a new similarity solution for the temperature field on an unsteady stretching surface by transforming the time-dependent thermal energy equation into an ordinary differential equation. Elbashbeshy and Bazid 18 presented an exact similarity solution for unsteady flow and heat transfer over a horizontal stretching surface and studied the effect of various governing parameters such as the Prandtl number and unsteadiness parameter which determine the velocity and temperature profiles and heat transfer coefficient. Later, Fang 19 extended the flow over a shrinking sheet to power law surface velocity and obtained the multiple solutions for certain mass transfer with controlling parameters. Tsai et al. 20 studied numerically the nonuniform heat source or sink effect on the flow and heat transfer from an unsteady stretching sheet through a quiescent fluid. The results showed that the heat transfer rate and the skin friction increase as the unsteadiness parameter increases, but, as the space- and temperature-dependent parameters for heat source/sink increase, the heat transfer rate and the skin friction decrease. Sajid and Hayat 21 investigated the effect of the MHD for two-dimensional and axisymmetric shrinking sheet. Later, Fang et al. 22 found that multiple solutions exist for a certain range of mass suction and unsteadiness parameters for the unsteady viscous flow over a continuously shrinking sheet. Recently, Adhikary and Misra [23] investigated the unsteady two-dimensional hydromagnetic flow and heat transfer of an incompressible viscous fluid. Very recently, Nik et al. [27] found that multiple solutions exist for a certain range of ratio of the shrinking velocity to the free stream velocity which again depends on the unsteadiness parameter for the unsteady stagnation point flow and heat transfer over a stretching/shrinking sheet

Due to its critical applications in the space technology, metallurgy, and pharmaceutical engineering industries, such as food processing technology, various hospital treatments, and polymer production, tremendous research has recently been conducted on the heat and mass transfer analysis of the flow over a stretching sheet. Furthermore, coupled heat and mass transfer problems involving homogeneous-heterogeneous reactions are important in a variety of engineering processes, thus they are receiving a lot of attention these days. As a result, possible applications can be identified in several systems, such as drying, temperature and moisture distribution throughout agricultural fields and fruit tree groves, and crop loss due to freezing. Hence, we extend the work Nik et al. [27] to the case of unsteady stagnation point flow of an incompressible viscous fluid by considering both stretching and shrinking sheets with suction or injection together with thermal and mass buoyancies, chemical reaction, Lorents force and variable heat source. Thus Nik et al. [27] becomes one of the special cases on this research. It is our belief that the results of this research will further provide deep insight into the effect of variable heat source and thermal buoyancy on Induced Magnetic Field on Unsteady Stagnation Point Flow of Mass and Heat Transfer over a Stretching/Shrinking Sheet with Suction or Injection. We shall establish the agreement between our work and previous related articles especiallyNik et al. [27]
A cautious assessment of previous analysis shows that noprevious attempt has been made to consider

the impacts of unsteady stagnation point flow of mass and heat transfer over a stretching/shrinking sheet with suction or injection in a stretchable porous device, despite thesignificance of the study to the manufacturing, biotechnology, computer technology, and general industrial expansion.Hence, the applications and various suggestions from previous studies motivate the present investigation as it relatesto technological improvement.

II. MATHEMATICAL FORMULATION

A. Problem Modelling

We consider a coupled heat and mass transfer by hydro - magnetic flow of a continuously moving vertical permeable surface in the presence of surface suction, heat generation/absorption effects, transverse magnetic field effects and chemical reactions.

The flow is assumed unsteady, laminar and the surface is maintained at a uniform temperature and the concentration species, and is assumed to be infinitely long. It is also assumed that the applied transverse magnetic Reynolds number is significant so that the induced magnetic field is considered. The porous layer is homogeneous and isotropic and it is heated and salted from below. Furthermore, the effects like activation energy, exponential temperature-dependent heat source/sink, and variable thermal and molecular diffusivity are also considered during mathematical formulation of the problem. The flow is characterized by temperature dependent viscousity and conductivity. In addition, there is no applied electric field and all of the Hall effect, viscous dissipation and Joule heating are neglected, thermo - physical properties are assumed constant except the density in the buoyancy terms of the momentum equation. The fluid is assumed to be Newtonian, electrically conducting and its property variations due to temperature and induced magnetic field are limited to fluid density. The density variation and the effects of the buoyancy are assumed to be negligible in the momentum equation (Boussinesq approximation). In addition, there is no applied electric field and all of the Hall effects and Joule heating are neglected. Under the aforementioned assumptions and after utilizing the necessary boundary layer approximations the full equation of motion for a two-dimensional flow in Cartesian form regarding continuity, momentum, energy, and concentration are given as

$$\frac{\partial u}{\partial x}+\frac{\partial v}{\partial y}=0 \tag{1}$$

$$\frac{\partial u}{\partial t}+u\frac{\partial u}{\partial x}+v\frac{\partial u}{\partial y}=U_\infty\frac{\partial U_\infty}{\partial x}+\nu\frac{\partial^2 u}{\partial y^2} -\frac{\sigma B_o^2(x)}{\rho_{n_f}}u+\frac{g\beta}{\rho_{nf}}(T-T_\infty)+\frac{g\beta_C}{\rho_{nf}}(C-C_\infty) \tag{2}$$

$$\frac{\partial T}{\partial t}+u\frac{\partial T}{\partial x}+v\frac{\partial T}{\partial y}=\frac{\kappa}{\rho_{n_f}c_p}\frac{\partial^2 T}{\partial y^2}+\left(\frac{\kappa u_w(x)}{\rho_{n_f}c_p x\nu}\right) \times\left[\frac{A^*(T_w-T_\infty)}{bx}(u-U)+B^*(T-T_\infty)\right] \tag{4}$$

$$\frac{\partial C}{\partial t}+u\frac{\partial C}{\partial x}+v\frac{\partial C}{\partial y}=\frac{D_m}{\rho_{n_f}}\frac{\partial^2 C}{\partial y^2} -\frac{k'\nu}{\tau\rho_{n_f}}\frac{\partial}{\partial y}\left((C-C_\infty)\frac{\partial T}{\partial y}\right)+k_r^2(C-C_\infty)^n \tag{5}$$

where u and v are velocity components in x and y directions; respectively, v is kinematic viscosity; $\kappa$is thermal diffusivity; T is fluid temperature.

The associated boundary conditions at the plate surface and far into the cold fluid may be written as:

$$u=u_w(x)+L\frac{\partial u(0)}{\partial y}, v=V_w(0), -k_{nf}\frac{\partial T(0)}{\partial y}=h(T_w-T), D_B\frac{\partial C(0)}{\partial y}=-\frac{D_T}{T_\infty}\frac{\partial T(0)}{\partial y} \tag{6}$$
$$u\to U_\infty, B_1\to B_e, T\to T_\infty, T\to T_\infty \text{as } y\to\infty$$

where $h$is the plate heat transfer coefficient,$T_w$is the plate temperature of the hot fluid at the left surface of the plate and k_{hnf} is the thermal conductivity coefficient.

The surface temperature and concentration of the sheet is assumed to vary by both the sheet and time, in accordance with $T_w(x,t)=T_\infty+bx(1-\alpha t)^{-2}$ and $C_w(x,t)=C_\infty+bx(1-\alpha t)^{-2}$ respectively. The wall temperature and concentration $T_w(x,t)$, $C_w(x,t)$ increases (reduces), if b is positive (negative) and is in proportion to x. Moreover, the amount of temperature and concentration increase (reduce) along the sheet increases with time. Here $v_w(t)=-v_0/\sqrt{(1-\alpha t)}$ at is the velocity of suction $v_0>0$ or blowing $v_0<0$. The expression for $U_w(x,t), v_w(t), C_w(x,t), \lambda(t), \kappa_r(t)$ is valid for time $t<\alpha^{-1}$.

B. Rate of Heat and Mass Transfer at the wall

The quantities of engineering interest are the Skin-Friction, local Nusselt number Nu and Sherwood

number Sh. These parameters characterize the wall heat and mass transfer rates,

The quantities skin-friction parameter, the plate surface temperature, Nusselt number and the Sherwood number can be easily computed. For local similarity case, integration over the entire plate is necessary to obtain the total skin-friction, total heat and mass transfer rate. These parameters characterize the wall nano heat and mass transfer rates, and are define similar to Mohamed and Ahmed (2018) as follows:

$$c_{f_x} = \frac{\tau_w}{\rho_{nf} U_w^2}, \quad Nu_x = \frac{x q_w}{k_{nf}(T_w - T_\infty)}, \quad Sh_x = \frac{x q_m}{D_m (C_w - C_\infty)} \tag{7}$$

where τ_w represents the skin friction along the surface, q_w the heat flux from the surface and are respectively given as

$$\tau_w = \mu \left[\frac{\partial u}{\partial y}\right]_{y=0}, q_w = -\kappa \left[\frac{\partial T}{\partial y}\right]_{y=0}, \quad q_m = -D_m \left[\frac{\partial C}{\partial y}\right]_{y=0} \tag{8}$$

where q_w and q_m, represents the heat and mass fluxes at the surface respectively.

III. METHOD OF SOLUTION

To seek for solution, we sought for a stream function $\psi(x, y, t)$ which must identically satisfied continuity equations, such that the stream function $\psi_{u,B}$ corresponding to velocity and magnetic field respectively, satisfies the continuity equation (1) and (2) automatically with

$$u = \frac{\partial \psi_u}{\partial y} \text{ and } v = -\frac{\partial \psi_u}{\partial x}. \tag{9}$$

A similarity solution of Equations (1) – (4) and (10) and (11) are obtained by defining an independent variable η and dependent variables f, θ and ϕ in terms of the stream function ψ as

$$\eta = y\sqrt{\frac{a}{\nu(1-\xi t)}}, \psi = \sqrt{\frac{a\nu}{1-\xi t}} x f(\eta) \tag{10}$$

The dimensionless temperature and concentration transformation are given as

$$\theta(\eta) = \frac{T - T_\infty}{T_w - T_\infty}, \qquad \phi(\eta) = \frac{C - C_\infty}{C_w - C_\infty}. \tag{11}$$

where η is similarity variable and ψ is stream function defined as $u = \partial\psi/\partial y$ and $v = -\partial\psi/\partial x$, thus we have

$$u = \frac{ax}{1-\xi t} f'(\eta), v = -\sqrt{\frac{a\nu}{1-\xi t}} f(\eta), \tag{12}$$

therefore, the mass transfer velocity V_w *at the wall* can take the form

$$V_w = -\sqrt{\frac{a\nu}{1-\xi t}} f_0, \tag{13}$$

where

$$T_w(x,t) = T_\infty + bx(1-\alpha t)^{-2}, \quad C_w(x,t) = C_\infty + bx(1-\alpha t)^{-2}$$

Applying (9)-(13) above, the system of equations (1)-(5) subject to (6) becomes

The full governing equations and the corresponding boundary conditions becomes

Therefore, the transformed governing equations together with the initial boundary conditions are

$$\frac{\partial^3 f(\eta)}{\partial \eta^3} - Ha \frac{\partial f(\eta)}{\partial \eta} - \left(\frac{\partial f(\eta)}{\partial \eta}\right)^2 + f(\eta)\frac{\partial^2 f(\eta)}{\partial \eta^2} - \alpha_1 \left(\frac{\partial f(\eta)}{\partial \eta} + \frac{\eta}{2}\frac{\partial^2 f(\eta)}{\partial \eta^2}\right) + Gr\left(\theta(\eta) + \mathrm{N}\phi(\eta)\right) + \lambda^2 = 0 \tag{14}$$

$$\frac{\partial^2 \theta(\eta)}{\partial \eta^2} - \Pr\left(\alpha_1 \frac{\eta}{2} - f(\eta)\right)\frac{\partial \theta(\eta)}{\partial \eta} + \left(A\frac{\partial f(\eta)}{\partial \eta} + A\theta(\eta)\right) = 0 \tag{15}$$

$$\frac{\partial^2 \phi(\eta)}{\partial \eta^2} - \beta \frac{\partial}{\partial \eta}\left(\phi(\eta)\frac{\partial \theta(\eta)}{\partial \eta}\right) - \alpha_1 \left(\frac{\eta}{2} - f(\eta)\right)\frac{\partial \phi(\eta)}{\partial \eta} + \delta_1 \phi(\eta)^n = 0 \tag{16}$$

$$f'(0) = 1 + N_1\sqrt{Re_x}\frac{\partial}{\partial \eta}\left(f'(0)\right), f(0) = S,$$

$$-Bi\sqrt{Re_x}\frac{\partial}{\partial \eta}\theta(0) = \left(1 - \theta(0)\right)$$

$$\frac{\partial}{\partial \eta}\left(\phi(0)\right) + Sr\frac{\partial}{\partial \eta}\left(\theta(-)\right) = 0$$

$$f'(\infty) \to \alpha_1, g'(\infty) \to \alpha_0, \theta(\infty) \to 0, \phi(\infty) \to 0$$

The wall rate transfer inn terms of skin-friction, Nusselt number and Sherwood number respectively becomes

$$\Longrightarrow c_f(Re_x)^{1/2} = \left[\left[\frac{\partial^2 f(\eta)}{\partial \eta^2}\right]\right]_{\eta=0} \quad (17)$$

$$\Longrightarrow Nu(Re_x)^{-1/2} = -\left[\frac{\partial \theta(\eta)}{\partial \eta}\right]_{y=0} \quad (18)$$

$$\Longrightarrow Sh(Re_x)^{-1/2} = -\left.\frac{\partial \phi(\eta)}{\partial \eta}\right|_{\eta=0}. \quad (19)$$

Where the local Reynolds number (Re_x) is define as

$$Re_x = xu_w/\nu_f = \frac{cx^2}{\nu_f(1-\alpha t)}$$

The flow governing Parameters are obtained as

$$\lambda = \frac{a}{c}, V = N\sqrt{\frac{c}{\nu_{nf}}}, r = \frac{T_w - T_\infty}{T_\infty},$$
$$N = \frac{\beta c(C_w - C_\infty)}{\beta t(T_w - T_\infty)}, \beta = \frac{(T_w - T_\infty)k_f}{T_r},$$
$$\alpha_1 = \frac{\alpha}{c}, Le = \frac{\mu_f}{Dm}, \frac{1}{Le} = \frac{D_m}{\mu_f}, \quad (20)$$
$$\frac{1}{Pr} = \frac{\kappa_f}{\mu_f c_{p_f}}, Gr = \frac{g\beta_T(T_w - T_\infty)}{\rho_{nf} c^2 x},$$
$$\delta = \frac{(1-\alpha t)k_r^2(C_w - C_\infty)^{n-1}}{c\rho_{nf}},$$

emerging flow governing paramerter. In the present analysis the fluid considered is flue gas.

IV. NUMERICAL SOLUTION OF THE PROBLEM

Numerical solutions to the transformed set of coupled, nonlinear, differential Eqs. (14)–(16) were obtained, utilizing a modification of the program suggested by Nachtsheim and Swigert. The higher order nonlinear partial differential equations are converted into first order simultaneous linear differential equations and then transformed to initial value problem. In this method the third-order nonlinear Eq. (8) and second order are converted to a system of first order differential equations and are solved numerically using Runge–Kutta fourth order method along with shooting technique.The system of equations has to be solved in the infinite domain $0 < \eta < \infty$. Grid-independence studies show that the computational domain $0 < \eta < \eta_\infty$ can be divided into intervals each of uniform step size which equals 0.02. This reduces the number of points between $0 < \eta < \eta_\infty$ without sacrificing accuracy. The value $\eta_\infty = 10$ was found to be adequate for all the ranges of parameters under consideration here. The solution for the non-magnetic and buoyancy case is chosen as an initial guess and the iterations using Euler scheme are continued till convergence within prescribed accuracy is achieved, with the corrections incorporated in subsequent iterative steps until convergence, which is used to obtain the values of our initial guesses.

As a result of the numerical calculations, the velocity, temperature and chemical species distributions for the flow are obtained and are displayed in Figs. 1–24 for different values of

A Results and discussion

For our analysis in this report, practical values for Prandtl number are chosen to be $Pr = 0.71$ which represents air and $Pr = 0.015$ for mercury at temperature 25℃ and one atmospheric pressure, Schmidt number (Sc) were chosen to be $Sc = 0.24, 0.62, 0.78, 2.62,$ representing diffusing chemical species of most common interest in air like H_2, H_2O, NH_3 and Propyl Benzene respectively. Attention is focused on positive values of the buoyancy parameters that is, Grashof number $Gr > 0$ (which corresponds to the cooling problem) and solutal Grashof number $Gc > 0$(which indicates that the chemical species concentration in the free stream region is less than the concentration at the boundary surface). In order to benchmark our numerical results, we have compared the values of $-Re_x^{1/2}C_f$for varying Deborah Number (β) when $n = 1.0, \gamma = 0.4$ and $Ha = 0.3$ when $Gr = Gc = 0$ with those results obtained by Abbasi et al. [36] and Hayat et al. [42], results are found to be in excellent agreement as demonstrated in Table 1.

Table 1: Comparative values of $-Re_x^{1/2}C_f$for varying b when $n = 1.0, \gamma = 0.4$ and $Ha = 0.3$.

β	Abbasi et al. [36]	Hayat et al. [42]	Current Result
0.0	0.88237	0.88237	0.88257044
0.3	1.00605	1.00605	1.00605498
0.6	1.11612	1.11612	1.11612186
1.0	1.24786	1.24786	1.24787382

B. Velocity distribution

The effect of flow governing parameters on velocity distribution were displayed in Figures 1 – 8. In Figure 1, the effect stretching parameter is observed to increase the velocity boundary layer of the fluid flow while from Figure 2, it was shown that Hartman number adversely affect velocity distribution. This Hartman number is known as Lorentz force which always act in opposite characteristic as velocity thereby brings about an opposing force which in turn reduces the bulk velocity. In Figure 3 and 4, thermal Grashof and buoyancy numbers are seen to aid velocity for cooling problem. It is also observed that for higher Grashof number, a peak exists close to the surface which indicate that maximum velocity occurs in the body of the fluid close to the surface. However, the velocity boundary layer reduces away from the surface with no significant changes far away from the plate surface. The effect of unsteadiness parameter was displayed in Figure 5. From this figure, we observed that as this unsteadiness parameter increase, the velocity distribution increases until at a threshold when the trend was reversed. While in Figure 6, an increase in space and fluidic heat generation ($A, B < 0$) reduces the velocity while heat absorption ($A, B > 0$) increases the velocity boundary layers. Figure 7 shows the variation of velocity distribution with Thermophoretic force. It was observed that thermophoretic parameter aided the velocity distribution. We displayed the effect of suction and injection parameter on velocity distribution in Figure 8 where we observed that for suction ($S < 0$), the velocity is increases while, for injection ($S > 0$) the velocity boundary layer decline. This is typical of what is experienced in a moving car with the windows wind down. Those whistling noises is due to air gushing in from outside there-by creating a kind of friction in the direction opposite to the direction of motion there-by decreasing the velocity of the car whereas, when the windows are rolled up, the friction on the car depend only on the shape and surface kind of the car.

C. Energy distribution

The effect of stretching parameter, Lorentz force, heat generation/absorption, thermophoretic Brownian motion and Eckert parameters and, Prandtl number on heat distribution in the boundary layer is shown in Figures 9 – 16. From these figures, we discovered that increase in stretching parameter decline the temperature of the flow while increase in Lorentz force (Hartman number) brings about increase in temperature as against the scenario in velocity field, as shown in Figure 9 and 10 respectively. This is because the opposition to velocity resulted into energy loss which is converted to heat thereby increases the bulk temperature of the flow. The unsteadiness parameter effect was displayed in Figure 11. The figure revealed that increase in unsteadiness parameter brings about increase in the thermal component of the flow. Both buoyancy ratio and thermal Grashof number were discovered to decrease the thermal component of the flow as displayed in Figures 12 and 13. While in Figure 14, an increase in space and fluidic heat generation ($A, B < 0$) reduces the flow bulk temperature while heat absorption ($A, B > 0$) increases the thermal boundary boundary layers. Also, at higher value of $A, B > 0$, a peak was observed on the profile which indicate that maximum temperature occurs in the body of the fluid close to the surface of the flow. The effect of thermophoretic parameters and convective heat transfer were shown in Figures 15 and 16 respectively. Increase in thermophoretic parameter was discovered to decrease the temperature of the flow while for convective heat transfer, temperature increases when heat moves from the solid surface to the fluid ($Bi > 0$) and decreases when heat moves from the fluid through the solid surface.

Table 2: Effect of flow governing parameters on wall transfer rate $f''(\eta)$, $\phi'(\eta)$and$\theta'(\eta)$

Parameters	$f''(\eta)$	$\phi'(\eta)$	$\theta'(\eta)$	Parameters	$f''(\eta)$	$\phi'(\eta)$	$\theta'(\eta)$
$\lambda = 0.0$	-0.11807	-0.83164	2.07911	$\delta_1 = -0.9$	-0.20811	-0.83626	2.09066
$\lambda = 0.2$	-0.13078	-0.77197	1.92991	$\delta_1 = -0.3$	-0.17970	-0.81365	2.03413
$\lambda = 0.4$	-0.11655	-0.68183	1.70458	$\delta_1 = 0.3$	-0.13078	-0.77197	1.92991
$\lambda = 0.6$	-0.05649	-0.58595	1.46487	$\delta_1 = 0.9$	-0.34702	-1.00177	2.50442
$Ha = 0.1$	-0.11025	-0.73524	1.83811	$S = -0.4$	0.19609	-0.85925	2.14813
$Ha = 0.5$	-0.18226	-0.88108	2.20270	$S = -0.2$	0.08497	-0.85220	2.13050
$Ha = 1.0$	-0.24115	-1.05296	2.63239	$S = 0.2$	-0.13078	-0.77197	1.92991
$Ha = 1.5$	-0.27469	-1.20455	3.01138	$S = 0.4$	-0.23829	-0.70103	1.75258
$\alpha_1 = 0.0$	-0.17966	-0.64642	1.61606	$Bi = -0.4$	-0.30870	-0.78318	1.95795

$\alpha_1 = 0.3$	0.00989	-1.05408	2.63519	$Bi = -0.2$	-0.23440	-0.78484	1.96209
$\alpha_1 = 0.6$	0.34924	-1.49296	3.73241	$Bi = 0.1$	-0.13078	-0.77197	1.92991
$\alpha_1 = 0.9$	-0.09998	-0.04787	0.11966	$Bi = 0.4$	-0.03907	-0.74601	1.86501
$N = 0.0$	-0.24739	-0.85658	2.14145	$Sr = 0.1$	-0.21313	-0.20766	2.07657
$N = 0.6$	-0.04702	-0.71764	1.79410	$Sr = 0.4$	-0.13078	-0.77197	1.92991
$N = 1.2$	0.07806	-0.64555	1.61388	$Sr = 0.8$	-0.04706	-1.43518	1.79398
$N = 2.4$	0.25365	-0.56027	1.40068	$Sr = 1.4$	0.05021	-2.31231	1.65165
$Gr = 0.2$	-0.25315	-1.33256	3.33140	$n = 0$	-0.18653	-0.83141	2.07853
$Gr = 0.5$	-0.13078	-0.77197	1.92991	$n = 1$	-0.17970	-0.81365	2.03413
$Gr = 0.8$	0.02196	-0.57012	1.42530	$n = 2$	-0.17997	-0.81306	2.03264
$Gr = 1.5$	0.34770	-0.37860	0.94651	$n = 3$	-0.18109	-0.81356	2.03390
$\beta = 0.0$	-0.17308	-0.80204	2.00510	$Sc = 0.30$	-0.04147	-0.65080	1.62700
$\beta = 0.3$	0.10822	-0.62851	1.57128	$Sc = 0.60$	-0.13078	-0.77197	1.92991
$\beta = 0.6$	0.70580	-0.41125	1.02811	$Sc = 0.94$	-0.17233	-0.81573	2.03932
$\beta = 1.1$	-0.29570	-0.90436	2.26089	$Sc = 2.60$	-0.22171	-0.84910	2.12274
$N_1 = 0.0$	-0.18609	-0.76628	1.91569	$Pr = 0.0015$	-0.57632	0.06450	-0.16124
$N_1 = 0.8$	-0.06923	-0.77830	1.94575	$Pr = 0.72$	-0.13078	-0.77197	1.92991
$N_1 = 1.6$	-0.04256	-0.78105	1.95262	$Pr = 4.0$	0.44350	-1.65692	4.14231
$N_1 = 3.2$	-0.02404	-0.78296	1.95739	$Pr = 6.0$	0.74183	-1.88241	4.70602

Table 3: Correlation between the flow parameter and the wall transfer rate

Parameters	$f''(\eta)$	$\phi'(\eta)$	$\theta'(\eta)$
λ	0.77	0.994806	-0.99481
Ha	-0.97966	-0.99919	0.999192
α_1	0.320564	0.284947	-0.28495
N	0.979312	0.957177	-0.95718
Gr	0.999586	0.891218	-0.89122
β	-0.0668	-0.18761	0.187612
δ_1	-0.51195	-0.58241	0.582414
N_1	0.838657	-0.83882	0.838818
S	-0.99998	0.969062	-0.96906
Bi	0.999168	0.929038	-0.92904
Sr	0.993172	-0.99848	-0.98691
n	0.648711	0.776863	-0.77686
Sc	-0.85292	-0.76977	0.769768
Pr	0.975296	-0.94304	0.943041

Table 3: Effect of Space Heat Source on wall transfer rate

Space Heat Source	$f''(\eta)$	$\phi'(\eta)$	$\theta'(\eta)$
As = -0.01, Bs = -0.01	-0.739312	0.210536	-0.526341
As = -0.11, Bs = -0.11	-0.811170	0.248939	-0.622347
As = 0.2, Bs = 0.2	-0.627368	0.080767	-0.201917
As = 0.4, Bs = 0.4	-0.493405	-0.120789	0.301973

D. Concentration distribution

In this section, the species concentrations were analysed with respect to various values of Hartman number, suction/injection parameter, unsteadiness parameter, buoyancy ratio, thermal Grashof number, Thermophoresis parameter, Soret and Schmidt numbers. Figure 17 shows the effect of Hartman number on the chemical species distribution. The figure showed that increase in Hartman number increases the chemical species boundary layers. While suction declines the chemical species distributions, injection increases the chemical species distributions as displayed in Figure 18. The unsteadiness parameter was discovered to enhance the chemical species distribution as unsteadiness parameter increases the

species boundary layer increases. In Figures 20, 21 and 24, the impact of buoyancy ratio, thermal Grashof number and Schmidt number were observed to decline the chemical species boundary layers. While the impact of thermophoretic parameter and Soret number were discovered to enhances the chemical boundary layers as displayed in Figures 22 and 23 respectively.

E. Rate of Heat and Mass Transfer at the wall

The flow rate at the wall in terms of skin friction $f''(0)$, heat flux $\theta'(0)$and concentration transfer at the wall $\phi'(0)$is displayed in Table 2. The effect of the flow governing parameters were explained using the data contained in the table. From the table, we discovered that unsteadiness parameter, Lewis number, thermophoretic parameter βwhereas, Soret number, stretching velocity, buoyancy ratio, Grashof number, magnetic inductance, nanofluid parameter, and reactivity parameter enhances the skin-friction. In this same vein, the effect of all these parameters on Skin-friction, Sherwood and Nusselt number analysed and explained using spearman correlation displayed in Table 3.

The Spearman correlation between two variables is equal to the Pearson correlation between the rank values of those two variables; while Pearson's correlation assesses linear relationships, Spearman's correlation assesses monotonic relationships (whether linear or not). If there are no repeated data values, a perfect Spearman correlation of +1 or −1 occurs when each of the variables is a perfect monotone function of the other, Wikipedia [28].The sign of the Spearman correlation indicates the direction of association between X (flow governing parameter) and Y (skin-friction, Nusselt and Sherwood number). If Y tends to increase when X increases, the Spearman correlation coefficient is positive. If Y tends to decrease when X increases, the Spearman correlation coefficient is negative. A Spearman correlation of zero indicates that there is no tendency for Y to either increase or decrease when X increases.

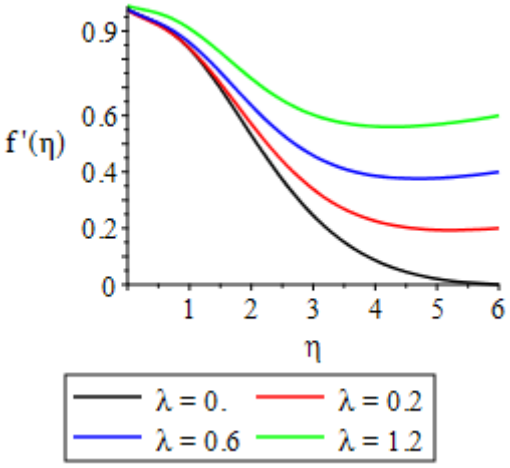

Figure 1: Graph of velocity for various values stretching parameter λ

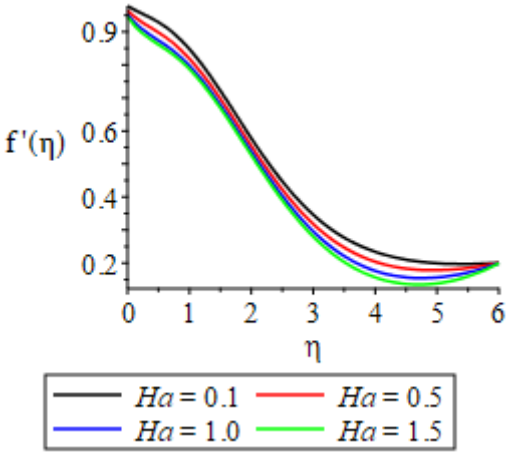

Figure 2: Graph of velocity for various values Hartmann Number Ha

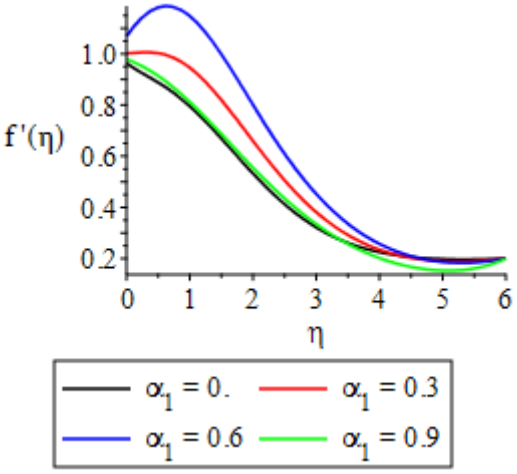

Figure 5: Graph of velocity for various values of unsteadiness parameter α_1

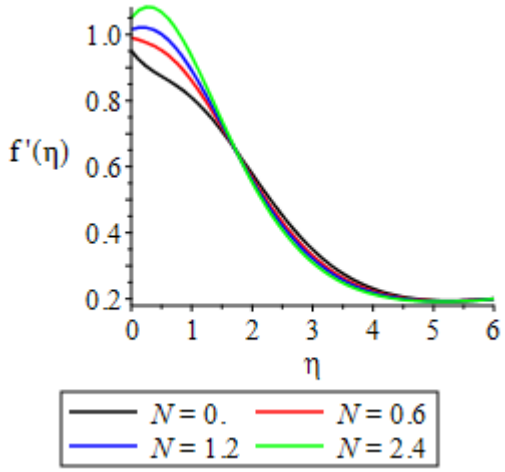

Figure 4: Graph of velocity for various values of Buoyancy parameters N

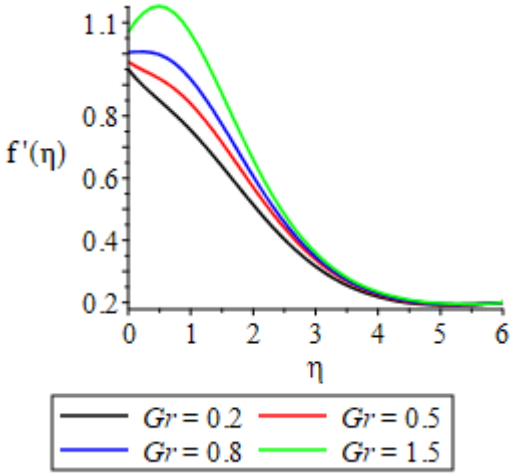

Figure 3: Graph of velocity for various values of Grashof number Gr

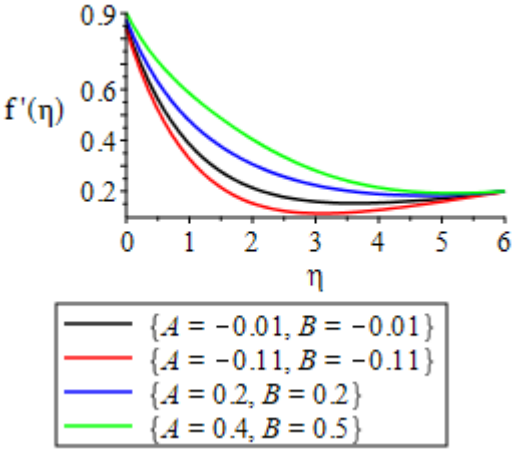

Figure 6: Graph of velocity for various values of space heat generation/absorption parameter A, B

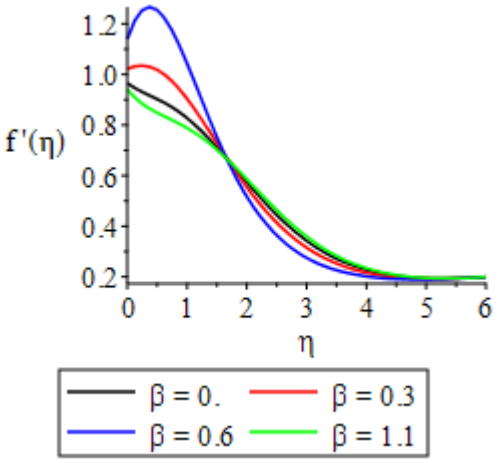

Figure 7: Shows the effect of thermophoretic force β on velocity distribution

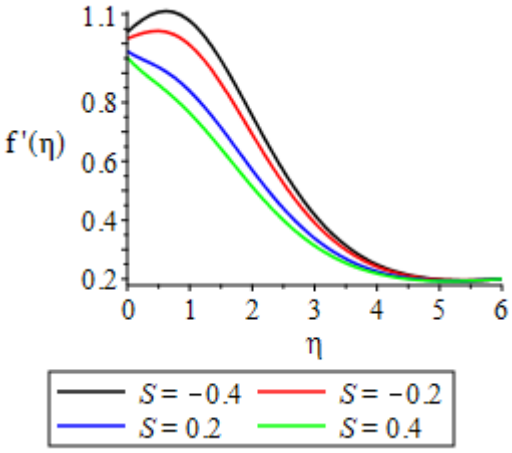

Figure 8: Graph of velocity for various values of injection/suction parameter S

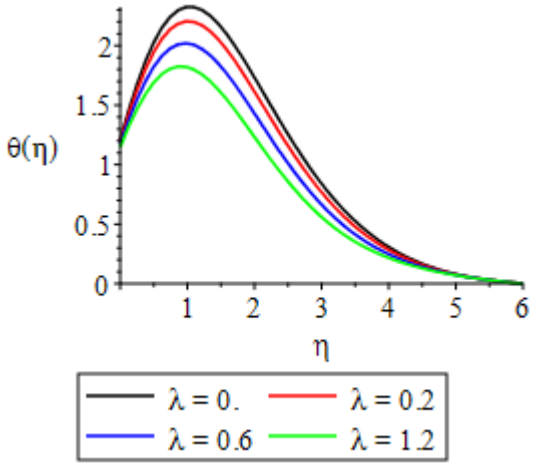

Figure 9: Graph of temperature for various values of stretching parameter λ

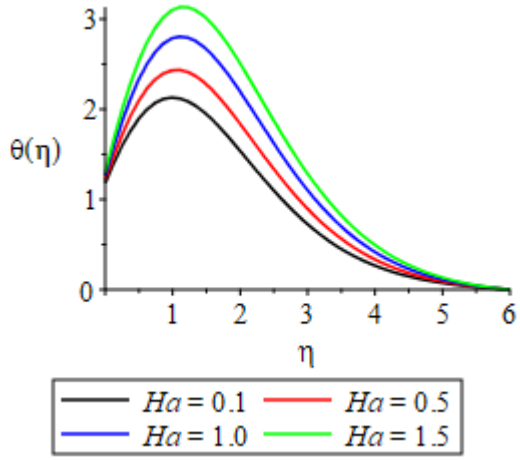

Figure 10: Graph of temperature for various values of Hartmann number Ha

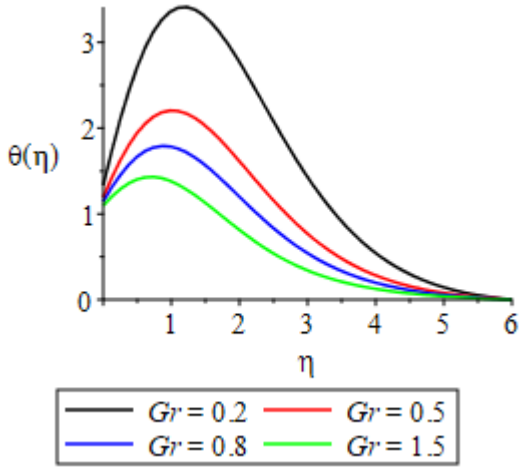

Figure 13: Graph of temperature for various values of thermal Grashof number Gr

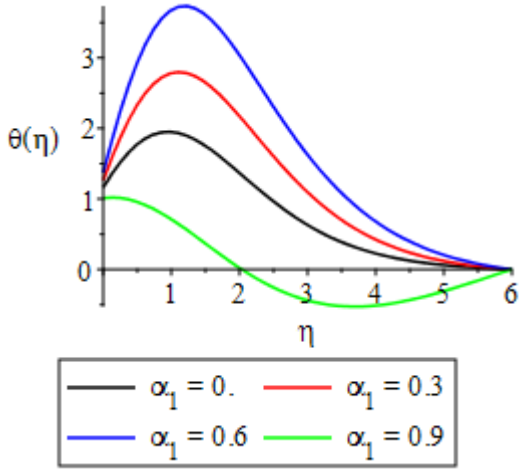

Figure 11: Graph of temperature for various values of unsteadiness parameter α_1

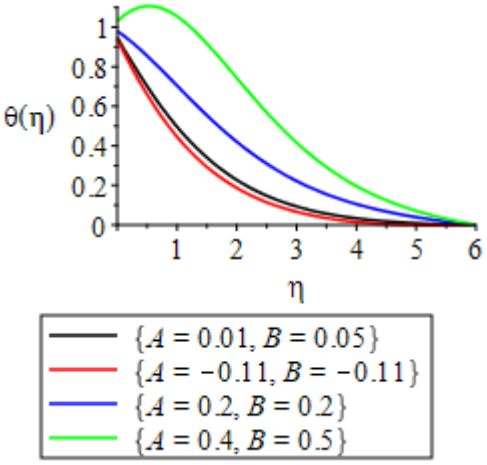

Figure 14: Graph of temperature for various values of space and fluidic heat generation.

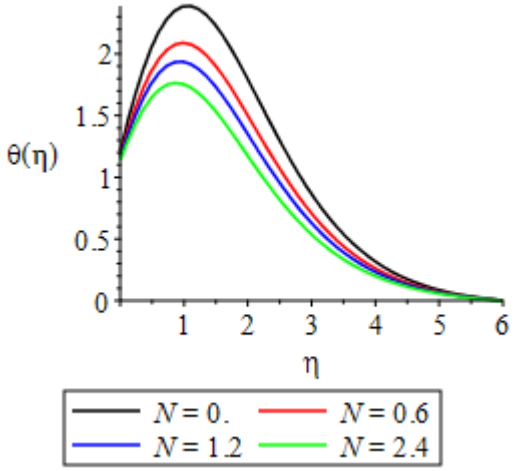

Figure 12: Graph of temperature for various values of buoyancy ratio N

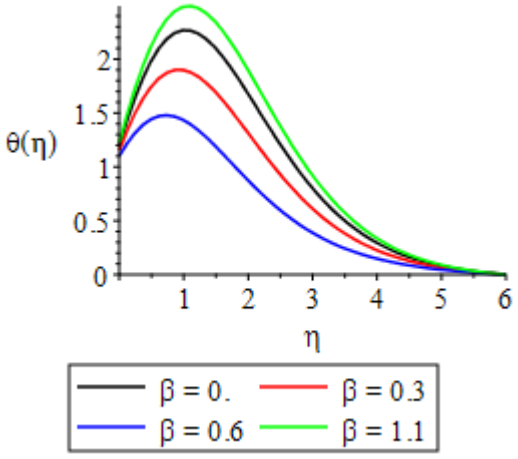

Figure 15: Graph of temperature for various values of Thermophoretic parameter β.

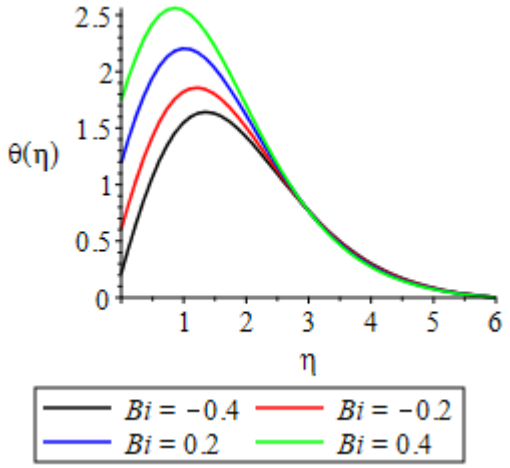

Figure 16: Graph of temperature for various values of convective heat parameter B_i

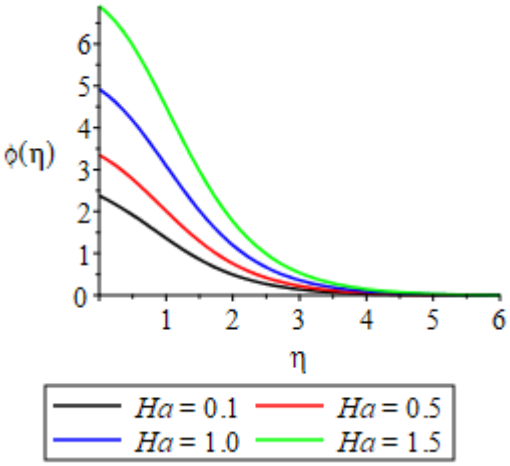

Figure 17: Graph of Chemical Specie for various values of Hartmann number Ha

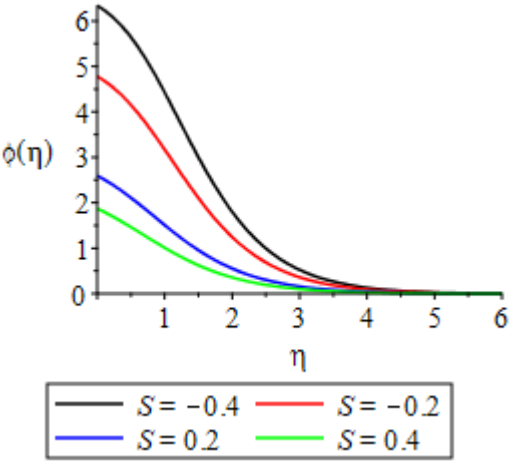

Figure 18: Graph of Chemical Specie for various values of suction/injection parameter S

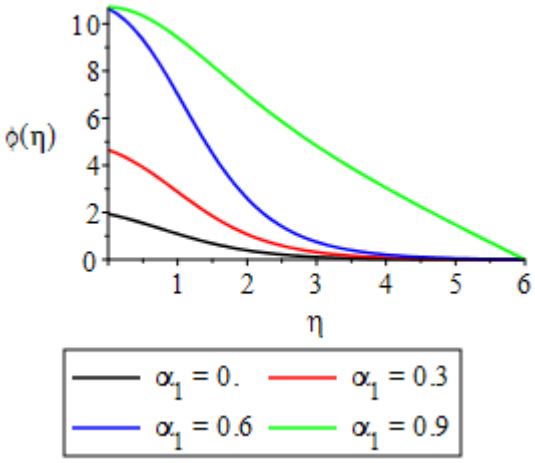

Figure 19: Graph of Chemical Specie for various values of unsteadiness parameter.

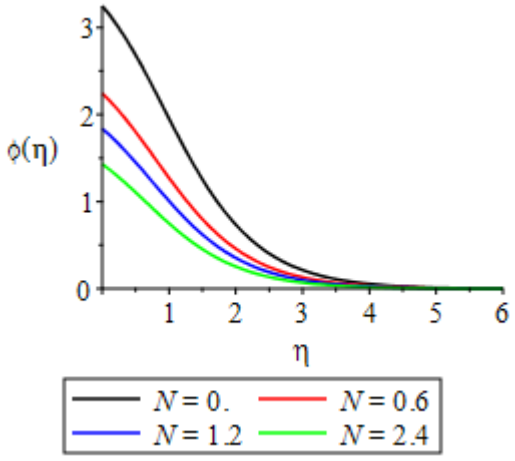

Figure 20: Graph of Chemical Specie for various values of buoyancy parameter N

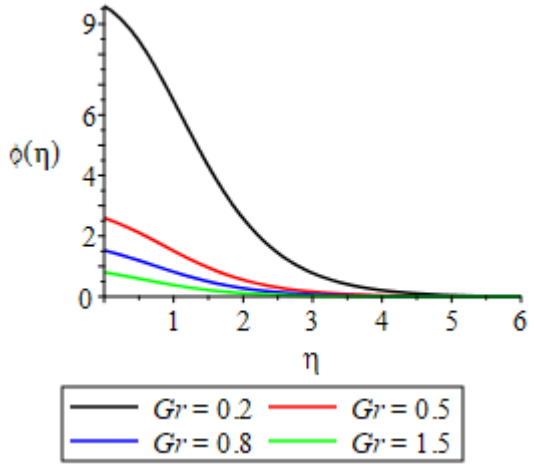

Figure 21: Graph of Chemical Specie for various values of thermal Grashof number Gr

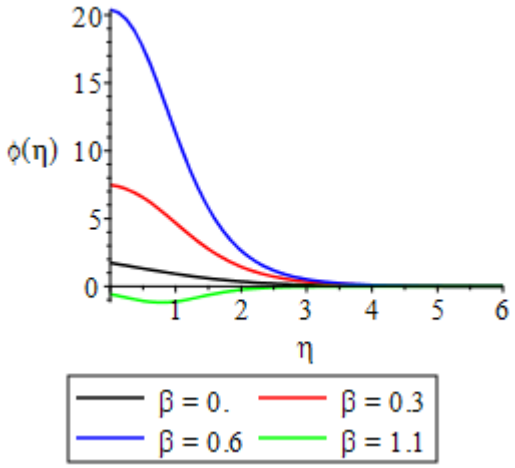

Figure 22: Graph of Chemical Specie for various of values thermophoretic parameter β

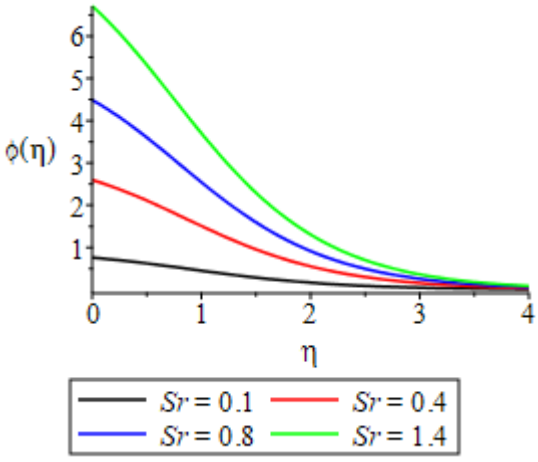

Figure 23: Graph of Chemical Specie for various values of Soret number Sr

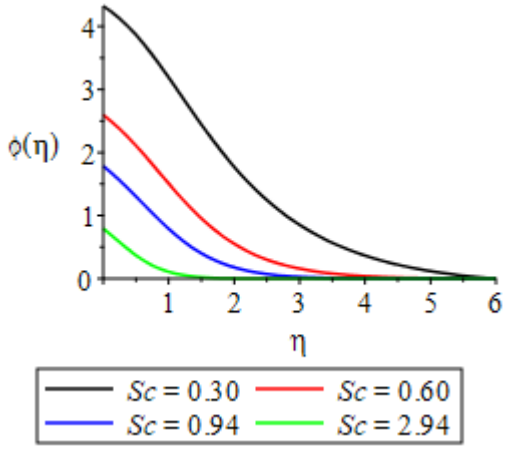

Figure 24: Graph of Chemical Specie for various values of Schmidt number Sc

CONCLUSION

Analysis of unsteady stagnation point flow of mass and heat transfer over a stretching/shrinking sheet with suction or injection in a stretchable porous device has been considered. Numerical solutions to the transformed set of coupled, nonlinear, differential equations were obtained, utilizing Runge–Kuta fourth order method along with shooting technique. As a result of the numerical calculations, the velocity, temperature and chemical species distributions for the flow are obtained and are displayed in figures and tables for different values flow governing parameters. From the result obtained and discussed above, the following were deduced:

- thermal Grashof and buoyancy numbers are discovered to aid velocity for cooling problem,
- unsteadiness parameter increases the velocity distribution until at a threshold when the trend was reversed,
- thermophoretic parameter aided the velocity boundary layers,
- for suction ($S < 0$), velocity increases with increases in Swhile, for injection ($S > 0$) the velocity boundary layer decline with increasing S,
- increase in stretching parameter decline the temperature of the flow
- while increase in Lorentz force (Hartman number) brings about increase in temperature as against the scenario in velocity field,
- increase in thermophoretic parameter was discovered to decrease the temperature of the flow,
- for convective heat transfer, temperature increases when heat moves from the solid surface to the fluid ($Bi > 0$) and decreases when heat moves from the fluid through the solid surface ($Bi < 0$),
- increase in Hartman number increases the chemical species boundary layers,
- suction declines the chemical species while, injection increases the chemical species distributions,
- increase in Thermal Grashof number result in increase in skin-friction,
- Hartman number generative chemical reaction suction and Scmidt number decline the velocity distributions.

DISCLOSURE

Sindi M Chigozie, Raphael E. Asibor and Akindele M. Okedoyepermanent address is as follows: Department of Mathematics, College of Science, Federal University of Petroleum Resources, Effurun, Department of Computer Science/Mathematics, Igbinedion University Okada, Edo State, Department of Mathematics, College of Science and Technology, Covenant University, Canaan Land, Ota, Nigeria

CONFLICTS OF INTEREST

The authors declare that there are no conflicts of interest regarding the publication of this article.

ACKNOWLEDGMENTS

The authors would like to express their gratitude to Covenant University, Ota, Ogun State, for providing enabling environment and research facilities.

REFERENCES

[1] D. Ingham, I. Pop (Eds.), Transport Phenomena in Porous Media, Oxford, 2005.

[2] D.A. Nield, A. Bejan, Convection in Porous Media, third ed., Springer, New York, 2006.

[3] Okedoye, A.M., Unsteady MHD Mixed Convection Flow past an Oscillating Plate with Heat Source/Sink, *J. Naval Architect. Marine Eng.*, vol. **11**, pp. 167–176, 2014.

[4] G. Ahmed, Muhammad Sajid, Thin-film flow of MHD third grade fluid in a porous space, Porous Media 12 (2009) 65–75.

[5] Masood Khan, R. Ellahi, Exact solution of oscillatory rotating flows of a generalized Oldroyd-B fluid through porous medium.: J. Porous Media. 12 (2009) 777–788.

[6] S. Abelman, E. Momoniat, T. Hayat, Steady MHD flow of a third-grade fluid in a rotating frame and porous space, Nonlinear Anal.: Real World Appl. 10 (6) (2009) 3322–3328.

[7] R. Ellahi, T. Hayat, F.M. Mahomed, The analytical solutions for magnetohydrodynamic flow of a third order fluid in a porous medium, Zeitschrift Fur Naturforschung A 64 (9) (2009) 531–539.

[8] T. Hayat, H.M. Mamboundou, F.M. Mahomed, A note on some solutions for the flow of a fourth grade fluid in a porous space, Nonlinear Anal.: Real World Appl. 10 (1) (2009) 368–374.

[9] M. Husain, T. Hayat, C. Fetecau, A note on decay of potential vortex in an Oldroyd-B fluid through a porous space, Nonlinear Anal.: Real World Appl. 10 (4) (2009) 2133–2138.

[10] T. Hayat, R. Naz, M. Sajid, On the homotopy solution for Poiseuille flow of a fourth-grade fluid, Commun. Nonlinear Sci. Numer. Simul. 15 (3) (2010) 581–589.

[11] T. Hayat, S. Nadeem, S. Asghar, A.M. Siddiqui, effects of hall current on unsteady flow of a second-grade fluid in a rotating system, Chem. Eng. Commun. 192 (2005) 1272–1284.

[12] T. Hayat, S. Mumtaz, Resonant oscillations of a plate in an electrically conducting rotating Johnson–Segalman fluid, Comput. Math. Appl. 50 (2005) 669–1676.

[13] T. Hayat, Exact solutions to rotating flows of a Burgers' fluid, Comput. Math. Appl. 52 (2006) 1413–1424.

[14] Z. Abbas, T. Javed, M. Sajid, N. Ali, Unsteady MHD flow and heat transfer on a stretching sheet in a rotating fluid, J. Taiwan Inst. Chem. Eng. 41 (2010) 644–650.

[15] N.T.M. Eldabe, Sallam N. Sallam, Mohamed Y. Abou-zeid, Numerical study of viscous dissipation effect on free convection heat and mass transfer of MHD non-Newtonian fluid flow through a porous medium, J. Egyptian Math. Soc. 20 (2012) 139–151

[16] Mohamed Abd El-Aziz 1 and Ahmed A. Afify (2018): Influences of Slip Velocity and Induced Magnetic Field on MHD Stagnation-Point Flow and Heat Transfer of Casson Fluid over a Stretching Sheet. Mathematical Problems in Engineering Volume 2018, Article ID 9402836, 11 pages https://doi.org/10.1155/2018/9402836.

[17] H. I. Andersson, J. B. Aarseth, and B. S. Dandapat, "Heat transfer in a liquid film on an unsteady stretching surface," *International Journal of Heat and Mass Transfer*, vol. 43, no. 1, pp. 69–74, 2000.

[18] E. M. A. Elbashbeshy and M. A. A. Bazid, "Heat transfer over an unsteady stretching surface," *Heat and Mass Transfer/Waerme-und Stoffuebertragung*, vol. 41, no. 1, pp. 1–4, 2004.

[19] T. G. Fang, "Boundary layer flow over a shrinking sheet with power-law velocity," *International Journal of Heat and Mass Transfer*, vol. 51, no. 25-26, pp. 5838–5843, 2008.

[20] R. Tsai, K. H. Huang, and J. S. Huang, "Flow and heat transfer over an unsteady stretching surface with non-uniform heat source," *International Communications in Heat and Mass Transfer*, vol. 35, no. 10, pp. 1340–1343, 2008.

[21] M. Sajid and T. Hayat, "The application of homotopy analysis method for MHD viscous flow due to a shrinking sheet," *Chaos, Solitons and Fractals*, vol. 39, no. 3, pp. 1317–1323, 2009.

[22] T. G. Fang, J. Zhang, and S. S. Yao, "Viscous flow over an unsteady shrinking sheet with mass transfer," *Chinese Physics Letters*, vol. 26, no. 1, Article ID 014703, 2009.

[23] S. D. Adhikary and J. C. Misra, "Unsteady two dimensional hydromagnetic flow and heat transfer of a fluid," *International Journal of Applied Mathematics and Mechanics*, vol. 7, no. 4, pp. 1–20, 2011.

[24] F. M. Ali, R. Nazar, N. M. Arifin, and I. Pop, "Unsteady shrinking sheet with mass transfer in a rotating fluid," *International Journal for Numerical Methods in Fluids*, vol. 66, no. 11, pp. 1465–1474, 2011.

[25] T. G. Fang, C. F. F. Lee, and J. Zhang, "The boundary layers of an unsteady incompressible stagnation point flow with mass transfer," *International Journal of Non-Linear Mechanics*, vol. 46, no. 7, pp. 942–948, 2011.

[26] K. Bhattacharyya, "Dual solutions in unsteady stagnation-point flow over a shrinking sheet," *Chinese Physics Letters*, vol. 8, Article ID 084702, 2011.

[27] N. M. A. Nik Long, M. Suali, A. Ishak, N. Bachok, and N. M. Arifin, "Unsteady stagnation point flow and heat transfer over a stretching/shrinking sheet," *Journal of Applied Sciences*, vol. 11, no. 20, pp. 3520–3524, 2011.

[28] https://en.m.wikipedia.org/wiki/Spearman's_rank_correlation_coefficient